SKIRTING AROUND THE NO-GO THEOREM IN MEASUREMENT-BASED QUANTUM COMPUTATION

THI HA KYAW
(B.Sc.(Hons.), NUS)

A THESIS SUBMITTED

FOR THE DEGREE OF MASTER OF SCIENCE
(PHYSICS) BY RESEARCH
DEPARTMENT OF PHYSICS
NATIONAL UNIVERSITY OF SINGAPORE

2015

Declaration of Authorship

I, THI HA KYAW, hereby declare that this thesis is my original work and it has been written by me in its entirety. I have duly acknowledged all the sources of information which have been used in the thesis.

This thesis has also not been submitted for any degree in any university previously.

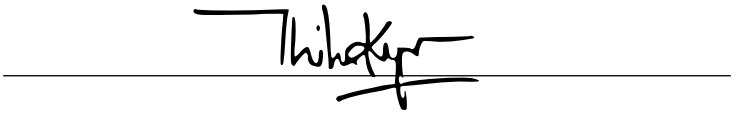

Thi Ha Kyaw

September 1, 2015

Acknowledgements

It is my upmost pleasure and gratitude to have my parents' unfailing love and support through ups and downs over the years to pursue my dream. I am also very grateful to have my soul-mate, Jumiati Wu, for her sacrifice and dedication in supporting me with completion of this thesis.

Physics-wise, I am very thankful to Dr. Ying Li for initiating this whole project and guiding me from the start to its fruitful publication. I also thank my supervisor, Professor Leong-Chuan Kwek for his boundless, unparrallel support and guidance. If there was an Oscar for outstanding supervisors, I am sure he would be collecting the prize every year. In addition, I would like to thank my main supervisor Professor Dagomir Kaszlikowski for his exceptional support. I have benefitted from numerous discussions/occasions with pepole in our research group at CQT. Without any preferrential order, they are Sai Vinjanampathy, Kwong Chang Jian, Davit Aghamalyan, Ewan Munro, and Wei Nie.

Contents

SKIRTING AROUND THE NO-GO THEOREM IN MEASUREMENT-BASED QUANTUM COMPUTATION

by THI HA KYAW

Summary

A cluster state cannot be a unique ground state of a two-body interacting Hamiltonian. Here, we propose the creation of a cluster state of logical qubits encoded in spin-1/2 particles by adiabatically weakening two-body interactions. The proposal is valid for any spatial dimensional cluster states. Errors induced by thermal fluctuations and adiabatic evolution within finite time can be eliminated ensuring fault-tolerant quantum computing schemes.

List of Figures

"Learn from yesterday, live for today, hope for tomorrow. The important thing is not to stop questioning."

— Albert Einstein

To my parents . . .

Chapter 1

Introduction

> "*He who sees things grow from the beginning will have the best view of them*".
>
> — Aristotle

Realization of a practical quantum computer remains a formidable and challenging task but yet it is an important dream to be pursued, despite evidence that seems to question its computational power. The current classical computer technology relies on gates and connecting wires to implement an algorithm. Therefore, it is natural to extend this model to the analogous quantum model. We now know that such a paradigm is possible and it is commonly known as the quantum circuit model [1]. In this model, every quantum algorithm is implemented through a quantum circuit, and the fundamental building blocks of such circuits are quantum gates, which can be categorized into single-qubit and two-qubit gates. If a set of quantum gates, be it single-, two-qubit or both, is sufficient to construct any arbitrary quantum circuit, we say that this set is universal

for quantum computation. For instance, an important universal set of quantum gates is composed of the controlled-NOT gate and arbitrary single-qubit quantum gates.

In order to design and build efficient quantum circuits that yield better performance than classical ones, it is crucial to exploit the unique features of quantum systems that optimize and enhance computations. It has been demonstrated that entanglement, one of the main pillars of quantum information processing, provides an important resource for the quantum speed-up over their classical counterparts [2, 3]. It is also likely that efficient quantum algorithms require a minimal amount of entanglement, otherwise the same quantum algorithm can also be simulated with classical computers. Typically, the input states to a typical quantum circuit usually take the form $|0\rangle \otimes |0\rangle \otimes \cdots |0\rangle$, which are not entangled. Thus, the entanglement needed for the quantum computation must be generated within the circuit itself. This means that some of the quantum gates, implemented with the quantum circuit model, should be able to generate entanglement necessary for the quantum speed-up. These gates are called quantum entangling gates. One familiar example is the controlled-NOT gate.

Small-scale realization of quantum circuits in various physical architectures has been studied extensively. These approaches include the manipulations through nuclear magnetic resonance [4], via atoms or ions in ion traps [5], via neutral atoms [6], implementation with cavity quantum electrodynamics [7] or circuit quantum electrodynamics [8, 9], the optical platform with linear or nonlinear optical devices [10], the manipulation of electrons or atoms in solid state devices

[11], and a "unique" approach to quantum information proposed in the quantum information roadmap [12]. Regardless of an approach we take, DiVincenzo has elegantly summarized five important criteria for any practical quantum computer [13], and each one of them has been carefully examined in the roadmap. To date, none of these systems is fully capable of realizing a large-scale quantum computer in the foreseeable future without any glitch. Each system presents its own unique advantages and challenges. One stumbling obstacle in many of these systems is that all quantum entangling gates cannot be implemented with high fidelity [14]. Thus, it is desirable to reduce the number of quantum entangling gates needed for quantum computation to its minimum.

To overcome some of the limitations, researchers have explored alternative pathways. Although these other paradigms are equivalent to the quantum circuit model in terms of computational power, they are very different in terms of real physical realization and implementation. Among the promising alternative paradigms are measurement-based quantum computing (MBQC) [15], topological quantum computing (TQC) [16] and adiabatic quantum computing (AQC) [17]. In this thesis, we mainly focus on the measurement-based quantum computing model as introduced by Raussendorf and Briegel in 2001 [15]. In particular, we have proposed a way [18] to skirt around the renowned no-go theorem in the MBQC, which is also the main theme of this thesis.

Chapter 2

The one-way quantum computation

"*Somewhere, something incredible is waiting to be known*".

— Carl Sagan

Measurement-based quantum computation (MBQC) or the one-way quantum computation [15] is an alternative paradigm, where desired quantum gate operations are obtained through projective measurements on individual physical qubits. These qubits structure themselves as computationally useful cluster states or highly entangled resource states. In this chapter, we define cluster states and show how to obtain single-qubit and two-qubit quantum gates via local measurements on individual qubits, thus giving rise to the universality of

MBQC. Lastly, we introduce stabilizers formalism, with exploration towards experimentally feasible physical systems are then outlined and discussed in the subsequent chapter.

2.1 Cluster states

Let us consider a simple lattice $\mathcal{L}_2$ shown in Fig.(2.1). A cluster state of the lattice structure is, in principle, attained if we position a spin-1/2 particle or a qubit in a state $|+\rangle$ at each vertex $V(\mathcal{L}_2)$, followed by a controlled-phase gate (CZ) application to every edge $E(\mathcal{L}_2)$. Physically, the $|+\rangle$ state can be created by preparing a qubit in its ground state and applying a $\pi/2$ pulse such that it is in equal superposition of the ground $|0\rangle$ and excited states $|1\rangle$, i.e., $|+\rangle = \frac{1}{\sqrt{2}}(|0\rangle + |1\rangle)$. To be precise, a cluster state is defined as

$$|\mathcal{C}\rangle_{\mathcal{L}_2} = \prod_{(c,t)\in E(\mathcal{L}_2)} CZ_{c,t} \bigotimes_{j\in V(\mathcal{L}_2)} |+\rangle_j, \tag{2.1}$$

where the subscripts c and t stand for control and target qubits. For instance, $CZ_{c,t} = |0\rangle_c\langle 0| \otimes \mathbb{1}_t + |1\rangle_c\langle 1| \otimes \sigma_t^z$, which means when the control qubit is in

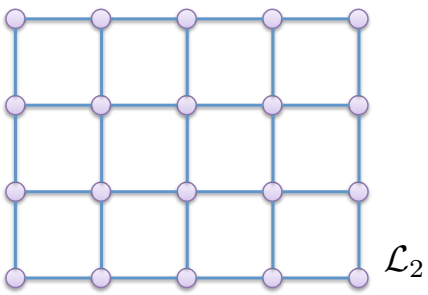

FIGURE 2.1: A simple two-dimensional square lattice.

state $|0\rangle$, CZ does not do anything to the target qubit, while the target qubit is phase-flipped when the control qubit is in state $|1\rangle$. From here onwards, we adopt the following notations throughout the thesis, unless otherwise is specified.

$$\mathbb{1} = \begin{pmatrix} 1 & 0 \\ 0 & 1 \end{pmatrix}; \ \sigma^x = \begin{pmatrix} 0 & 1 \\ 1 & 0 \end{pmatrix}; \ \sigma^y = \begin{pmatrix} 0 & -i \\ i & 0 \end{pmatrix}; \ \sigma^z = \begin{pmatrix} 1 & 0 \\ 0 & -1 \end{pmatrix}. \quad (2.2)$$

The above matrices are written in the basis of $|0\rangle = (1,0)^{\mathrm{T}}$ and $|1\rangle = (0,1)^{\mathrm{T}}$, where T stands for the transpose.

To grasp the idea of cluster states, we shall investigate its simplest form, a two-qubit cluster state, as shown in Fig.(2.2) (a). Instead of looking at the whole square lattice $\mathcal{L}_2$, let us focus at two sites linked with an edge. From the definition, Eq.(2.1), we have

$$\begin{aligned} |\mathcal{C}_2\rangle &= CZ_{1,2}|+\rangle_1|+\rangle_2 = CZ_{1,2}\frac{[|0\rangle_1|+\rangle_2 + |1\rangle_1|+\rangle_2]}{\sqrt{2}} \\ &= \frac{1}{\sqrt{2}}[|0\rangle_1|+\rangle_2 + |1\rangle_1|-\rangle_2]. \end{aligned} \quad (2.3)$$

Similarly, if we exchange the control and target qubits in CZ, we have

$$|\mathcal{C}_2\rangle = CZ_{2,1}|+\rangle_1|+\rangle_2 = \frac{1}{\sqrt{2}}[|+\rangle_1|0\rangle_2 + |-\rangle_1|1\rangle_2]. \quad (2.4)$$

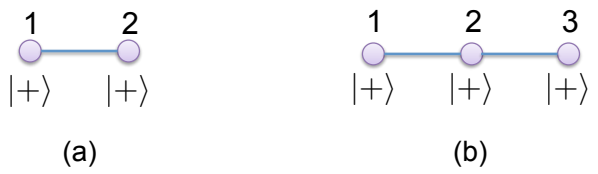

FIGURE 2.2: (a) Two-qubit cluster state, (b) three-qubit cluster state.

Therefore, $|\mathcal{C}_2\rangle$ is symmetric under the control and target qubits exchange. We can contiune our analysis by adding an additional third qubit as shown in Fig.(2.2) (b) and arrive at

$$|\mathcal{C}_3\rangle = CZ_{2,3}CZ_{2,1}|+\rangle_1|+\rangle_2|+\rangle_3 = \frac{1}{\sqrt{2}}[|+\rangle_1|0\rangle_2|+\rangle_3 + |-\rangle_1|1\rangle_2|-\rangle_3]. \quad (2.5)$$

We can continue this calculation/analysis in accordance with Eq.(2.1) and get an exact expression for cluster states of any lattice structure. However, we are interested in quantum computations done on cluster states, rather than classification of different cluster states. Therefore, we shall move on to discuss the quantum computational aspects of cluster states.

2.2 Universal MBQC

In classical computers, not-AND (NAND) gate is considered as a universal gate since collection of NAND gates in various combinations can give rise to all the required classical logic gates for a computing algorithm. Likewise, a universal quantum computation is achieved if either an arbitrary single-qubit gate operation and controlled-NOT (CNOT) are realized or a specific single-qubit gate and an arbitrary two-qubit entangling gate are achieved. Since the former is easier achieved, we show the universality of MBQC by attaining general one-qubit gate and two-qubit CNOT gate [1].

2.2.1 General one-qubit gate

Let us revisit the two-qubit cluster state that we have discussed in the previous section. It has an equivalent quantum circuit model as shown in Fig.(2.3) (a). Instead of looking at it as two stationary $|+\rangle$ states under a CZ operation, we can take it as two $|+\rangle$ states being sent through two different quantum channels (black colored straight lines) and they are performed a CZ gate in the middle of their propagation. A resultant cluster state is then spit out at the channel ends.

We can go one step further from Fig.(2.3) (a) and consider a case when the qubit 1 is an arbitrary input state $|\text{in}\rangle = a|0\rangle + b|1\rangle$, where a and b are arbitrary complex numbers, and the qubit-2 remains $|+\rangle$, such as shown in Fig.(2.3) (b). Then, we perform CZ gate, followed by a general projective measurement on the qubit-1,

$$\hat{O}(\varphi) = (\cos\varphi)\sigma_1^x + (\sin\varphi)\sigma_1^y, \tag{2.6}$$

The operator $\hat{O}$ has eigenvalues ± 1 with corresponding eigenvectors $|v_\pm\rangle = (|0\rangle \pm e^{i\varphi}|1\rangle)/\sqrt{2}$. Thus, if we perform the projective measurement ($\hat{O}$) on the qubit-1,

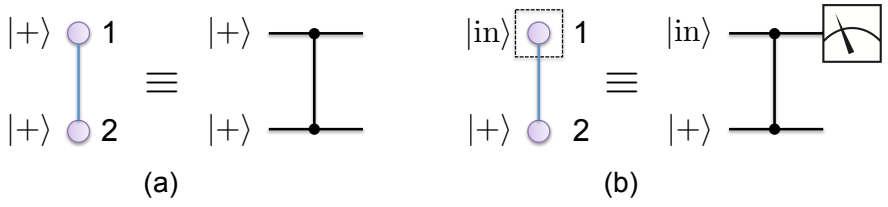

FIGURE 2.3: (a) Two-qubit cluster state (left) and its equivalent quantum circuit (right), (b) an arbitrary input $|\text{in}\rangle$ state entangled with a $|+\rangle$ state undergoes a general projective measurement (left, measurement is denoted by a dotted box) and its equivalent quantum circuit (right, measurement is denoted by a solid box).

we expect to have two different outcomes, depending on measurement outcomes, the eigenvalues $\pm 1 = (-1)^{m_1}, m_1 \in \{0, 1\}$. Before the measurement, we have, from Fig.(2.3) (b), the entangled state $|\psi\rangle_{1,2} = a|0,+\rangle + b|1,-\rangle$. Suppose we get measurement outcome $m_1 = 0$. This means the state of qubit-2 becomes

$$\begin{aligned} |\psi\rangle_2 = \langle v_+|\psi\rangle_{1,2} &= \frac{1}{\sqrt{2}}(\langle 0| + e^{-i\varphi}\langle 1|)_1(a|0,+\rangle + b|1,-\rangle)_{1,2} \\ &= \frac{1}{\sqrt{2}}(a|+\rangle + be^{-i\varphi}|-\rangle)_2 \\ &\sim e^{-i\varphi/2}(e^{i\varphi/2}a|+\rangle + be^{-i\varphi/2}|-\rangle) \\ &= He^{i\varphi\sigma^z/2}|\text{in}\rangle, \end{aligned} \tag{2.7}$$

where H is the Hadamard gate

$$H = \frac{1}{\sqrt{2}}\begin{pmatrix} 1 & 1 \\ 1 & -1 \end{pmatrix}. \tag{2.8}$$

Similarly, for the outcome $m_1 = 1$, we have

$$\begin{aligned} |\psi\rangle_2 = \langle v_-|\psi\rangle_{1,2} &= \frac{1}{\sqrt{2}}(\langle 0| - e^{-i\varphi}\langle 1|)_1(a|0,+\rangle + b|1,-\rangle)_{1,2} \\ &\sim e^{-i\varphi/2}(e^{i\varphi/2}a|+\rangle - be^{-i\varphi/2}|-\rangle) \\ &= He^{i\varphi\sigma^z/2}\sigma^z|\text{in}\rangle. \end{aligned} \tag{2.9}$$

Combining both results, we have $|\psi\rangle_2 = (He^{i\varphi\sigma^z/2}(\sigma^z)^{m_1})|\text{in}\rangle$. In other words, the input state, which was at location 1, has been teleported to location 2, with some gate operations done, depending on the measurement outcome, m_1.

To achieve a general one-qubit gate, we add three additional qubits as shown in

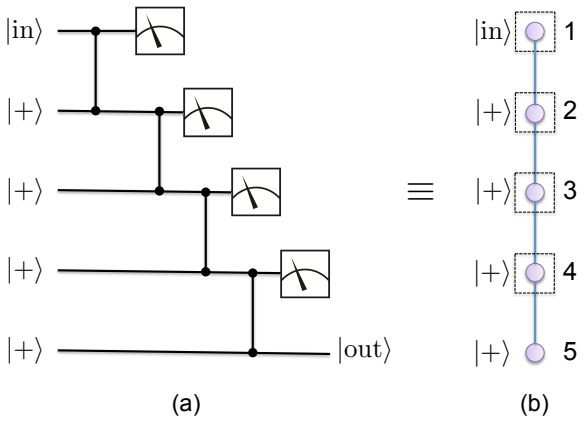

FIGURE 2.4: (a) Quantum circuit model to attain a general one-qubit unitary gate. Time flows from left to right. (b) Equivalent setup of the general one-qubit unitary gate in one-dimensional chain of cluster state. Time flows from top to bottom.

Fig.(2.4). Output state at location 5 after four projective measurements is given by

$$|\text{out}\rangle = (He^{i\varphi_4\sigma^z/2}(\sigma^z)^{m_4})(He^{i\varphi_3\sigma^z/2}(\sigma^z)^{m_3}) \times (He^{i\varphi_2\sigma^z/2}(\sigma^z)^{m_2})(He^{i\varphi_1\sigma^z/2}(\sigma^z)^{m_1})|\text{in}\rangle = U^1|\text{in}\rangle, \quad (2.10)$$

where

$$U^1 = (\sigma^z)^{m_1+m_3}(\sigma^x)^{m_2+m_4} \times \exp\left(i(-1)^{m_1+m_3}\frac{\varphi_4}{2}\sigma^x\right)\exp\left(i(-1)^{m_2}\frac{\varphi_3}{2}\sigma^z\right)\exp\left(i(-1)^{m_1}\frac{\varphi_2}{2}\sigma^x\right), \quad (2.11)$$

is a general one-qubit gate that is able to rotate any vector on the Bloch sphere to an arbitrary direction. Here, we assume $\varphi_1 = 0$ and we have made use of the following identities: $H\sigma^z = \sigma^x H$ and $\sigma^x\sigma^z = -\sigma^z\sigma^x$.

So far, we have considered a one-dimensional chain cluster states. In oder to

achieve a two-qubit gate, we need two-dimensional cluster states. The simplest CNOT gate configuration is shown in Fig.(2.5) and it needs four qubits located across a two-dimensional lattice.

2.2.2 Controlled-NOT gate

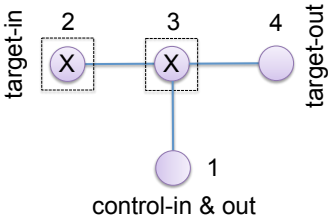

FIGURE 2.5: Controlled-NOT gate. Input and output are located on the same cluster qubit-1, and two σ^x (X) measurements are performed on qubit-2 and 3.

From the previous prescription, Eq.(2.1), the cluster state corresponding to Fig.(2.5), can be written as

$$
\begin{aligned}
|\psi\rangle_{1,2,3,4} &= CZ_{4,3}CZ_{1,3}CZ_{2,3}[(a|0\rangle + b|1\rangle)_1(c|0\rangle + d|1\rangle)_2|+\rangle_3|+\rangle_4] \qquad (2.12)\\
&= a|0\rangle_1(c|0,+\rangle + d|1,-\rangle)_{2,3}|0\rangle_4 + b|1\rangle_1(c|0,-\rangle + d|1,+\rangle)_{2,3}|0\rangle_4 + \\
&\quad a|0\rangle_1(c|0,-\rangle + d|1,+\rangle)_{2,3}|1\rangle_4 + b|1\rangle_1(c|0,+\rangle + d|1,-\rangle)_{2,3}|1\rangle_4.
\end{aligned}
$$

When we perform σ^x-measurement (X) onto qubits-2 and 3, i.e., projection with the basis $|\pm\rangle = (|0\rangle \pm |1\rangle)/\sqrt{2}$, we have four different possbile scenarios, which are listed in the Table.(2.1), depending on their respective eigenvalues $(-1)^{m_2}$ and $(-1)^{m_3}$, while $m_2, m_3 \in \{0, 1\}$. For the case A, we have $m_2 = 0$ and $m_3 = 0$.

That means, after the measurements, we have

$$\begin{aligned} |\psi\rangle_{1,4} &= {}_{2,3}\langle +,+| \cdot |\psi\rangle_{1,2,3,4} \\ &= a|0\rangle_1(c|0\rangle + d|1\rangle)_4 + b|1\rangle_1(c|1\rangle + d|0\rangle)_4 \\ &= U^2_{1,4}(a|0\rangle + b|1\rangle)_1(c|0\rangle + d|1\rangle)_4, \end{aligned} \tag{2.13}$$

where $U^2_{1,4}$ is a CNOT gate with the control qubit-1 and the target qubit-4. From the above simple analysis, we see that the target qubit information which was originally located at location 2 has just been teleported to location 4, and we attain the desired CNOT gate, in accordance with the control qubit-1. Similarly, we have

$$|\psi\rangle_{1,4} = U^2_{1,4}(a|0\rangle + b|1\rangle)_1(c|1\rangle + d|0\rangle)_4, \quad \text{(case B)} \tag{2.14}$$

$$|\psi\rangle_{1,4} = U^2_{1,4}(a|0\rangle + b|1\rangle)_1(c|0\rangle - d|1\rangle)_4, \quad \text{(case C)} \tag{2.15}$$

$$|\psi\rangle_{1,4} = U^2_{1,4}(a|0\rangle + b|1\rangle)_1(c|1\rangle - d|0\rangle)_4. \quad \text{(case D)} \tag{2.16}$$

In general, we can summarize all the four cases as

$$|\text{out}\rangle = U^2_{c,t}(\sigma^x_t)^{m_3}(\sigma^z_t)^{m_2}(a|0\rangle + b|1\rangle)_c(c|0\rangle + d|1\rangle)_t. \tag{2.17}$$

	m_2	m_3
A	0	0
B	0	1
C	1	0
D	1	1

TABLE 2.1: Four different cases A-D are possible, depending on the outcomes m_2 and m_3.

2.3 Stabilizers

We have been discussing our computationally useful resource states in the state vector notation all along. While the former allows us to see explicit structure of the cluster states, it is rather convenient to adopt an operator formalism, with which one can write down a system Hamiltonian, useful for experimental realizations.

A cluster state is defined, from Eq.(2.1), to be a resultant state after series of controlled-phase (CZ) gate operations between initial states $|+\rangle^{\otimes N}$, where N is the total number of qubits. Here, we recall some properties of the CZ gate.

$$CZ_{c,t}\sigma_c^x CZ_{c,t}^\dagger = \sigma_c^x\sigma_t^z, \tag{2.18}$$

$$CZ_{c,t}\sigma_t^x CZ_{c,t}^\dagger = \sigma_t^x\sigma_c^z, \tag{2.19}$$

$$CZ_{c,t}\sigma_c^z CZ_{c,t}^\dagger = \sigma_c^z, \tag{2.20}$$

$$CZ_{c,t}\sigma_t^z CZ_{c,t}^\dagger = \sigma_t^z. \tag{2.21}$$

Let us revisit the three-qubit cluster state as shown in Fig.(2.6) (a). From the definition, Eq.(2.1), the cluster state is given by $|\mathcal{C}_3\rangle = CZ_{1,2}CZ_{2,3}|+,+,+\rangle_{1,2,3}$.

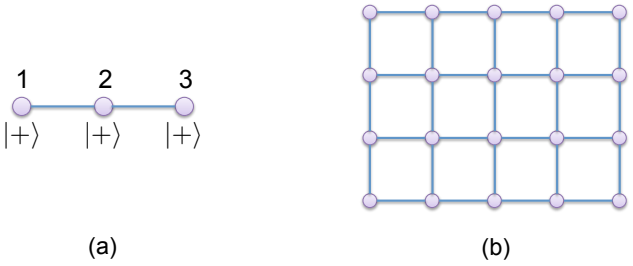

FIGURE 2.6: (a) Three-qubit cluster state. (b) A simple square lattice.

Since $|\mathcal{C}_3\rangle$ is composed of $|+\rangle^{\otimes 3}$, $|\mathcal{C}_3\rangle$ is invariant under σ_2^x, which is the first equality in Eq.(2.22). And, we then invoke an identity operator: $\mathbb{1} = CZ_{2,3}^{\dagger} CZ_{2,3}$, giving rise to the third equality. With the aid of Eq.(2.18), we arrive at the fourth equality. We can continue the same step, and we finally arrive at the final equality in Eq.(2.22).

$$\begin{aligned} CZ_{1,2}CZ_{2,3} &= CZ_{1,2}CZ_{2,3}\sigma_2^x = CZ_{1,2}CZ_{2,3}\sigma_2^x CZ_{2,3}^{\dagger} CZ_{2,3} \\ &= CZ_{1,2}\sigma_2^x\sigma_3^z CZ_{2,3} = \sigma_2^x\sigma_1^z\sigma_3^z CZ_{1,2}CZ_{2,3}. \end{aligned} \tag{2.22}$$

Intuitively, Eq.(2.22) means that phase-flip errors at qubit-1, qubit-3, and bit-flip error at qubit-2 do not change the state $|\mathcal{C}_3\rangle$, i.e., $\sigma_2^x\sigma_1^z\sigma_3^z|\mathcal{C}_3\rangle = |\mathcal{C}_3\rangle$. Thus, $\sigma_2^x\sigma_1^z\sigma_3^z$ stabilizes $|\mathcal{C}_3\rangle$. Likewise, we find $\{\sigma_2^x\sigma_1^z\sigma_3^z, \sigma_3^x\sigma_2^z, \sigma_1^x\sigma_2^z\}$ is a set of stabilizers for a particular graph of the three-qubit cluster state, Fig.(2.6) (a). In general, given a graph $\mathcal{L}$,

$$\left(\sigma_u^x \prod_{v\in nb(u)} \sigma_v^z\right) |\mathcal{C}\rangle_{\mathcal{L}} = |\mathcal{C}\rangle_{\mathcal{L}}, \tag{2.23}$$

uniquely defines the cluster state, $\forall u \in V(\mathcal{L})$, and $nb(u)$ represents neighbours of u. An alternative physical interpretation from Eq.(2.23) is that a cluster state is an eigenvector of the operator $\left(\sigma_u^x \prod_{v\in nb(u)} \sigma_v^z\right)$ with an eigenvalue $+1$. We also notice that the operators associated with different vertices commute. For instance in the three-qubit cluster state, $\sigma_2^x\sigma_1^z\sigma_3^z, \sigma_3^x\sigma_2^z$, and $\sigma_1^x\sigma_2^z$ commute with

each other. Hence, if a system Hamiltonian is in the following form

$$H = -\sum_{u \in V} \sigma_u^x \prod_{v \in nb(u)} \sigma_v^z, \tag{2.24}$$

then $|\mathcal{C}\rangle_{\mathcal{L}}$ is the unique ground state of the system H, with an energy gap. However, such Hamiltonian is, in general, not a two-body interacting system. If we impose Eq.(2.24) onto the simplest two-dimensional square lattice of Fig.(2.6) (b), we arrive at a five-body interacting Hamiltonian, which is unfavourable since it is formidable for an experimental realization.

Chapter 3

MBQC on two-body interacting qubits with adiabatic evolution

> "*Nothing in life is to be feared, it is only to be understood. Now is the time to understand more, so that we may fear less*".
>
> — Marie Curie

As we have learned from the previous chapter, the creation of a cluster state or an appropriate highly entangled resource state [19] is a holy grail of measurement-based quantum computation [15, 20, 21]. Ideally, we would like to obtain cluster states by cooling naturally occurring systems down to their unique ground state, thereby avoiding any entangling gate operation. To recall, one of the resource states for the MBQC is the ground state of spin-1/2 particles with 5-body interactions [see Fig.(2.6) (b)]. In general, many other configurations with k-body

interactions where $k \geq 3$ [22, 23] are also possible. However, there exists a no-go theorem that forbids a unique ground state of a two-body nearest-neighbor interacting Hamiltonian to be a cluster state [24].

Many proposals exist to overcome this obstacle or at least to skirt around this no-go theorem. For instance, ground state of two-body interacting Hamiltonian, such as that of the one-dimensional Affleck, Kennedy, Lieb and Tasaki (AKLT) model of spin-1 particles [25, 26] or the two-dimensional AKLT model of spin-3/2 particles, gives rise to cluster state, after suitable projective measurements. One should bear in mind that the particles interaction in these systems should be immediately turned off in order to circumvent degradation of quantum correlations, required for the quantum information processing [25–31]. The spontaneous switching-off is sometimes not needed, when the system evolves with an always-on periodically driven interactions [32, 33]. Otherwise, an adiabatic switching-off is commenced to isolate the quantum information to the edge states [34].

In this project, we investigate MBQC on systems of two-body interacting spin-1/2 particles via adiabatic evolution, since such systems, compared to systems with higher spins and many-body interactions, are generally better suited for experimental implementation [35]. For example, cluster state of the five-body interacting Hamiltonian can be approximated with two-body interactions via weak perturbations [36], which mean a small energy gap between the ground and first excited states. As a result, such system needs to be cooled down to a sufficiently low operating temperature, depending on the size of the energy gap. Here, we concentrate cluster states by adiabatically evolving the ground state

of two-body interacting spin-1/2 particles with a built-in energy gap protection, which allows us to operate at a higher temperature environment.

3.1 Motivation of cluster state concentration via adiabatic weakening

The main motivation of our proposal comes from adiabatic quantum computing (AQC) [17, 37, 38], but it differs from the standard AQC as follows. A system in the AQC is initially prepared in the ground state of a simple Hamiltonian. By adiabatically evolving the Hamiltonian to a target Hamiltonian, the final desired state is obtained at the end. Moreover, the instantaneous ground states during the evolution usually need to be protected by a finite energy gap [39]. Creation of cluster states via the standard AQC is impossible as we need a target Hamiltonian whose unique ground state is the cluster state. While a cluster state is never a unique ground state of any two-body interaction Hamiltonian (the no-go theorem), it can still be one of the degenerate ground states. By gradually weakening the interactions of a two-body Hamiltonian, we propose that the system could finally achieve a cluster state as one of the degenerate ground states. We also notice the disapperance of the system energy gap at the end of the adiabatic evolution when a cluster state of logical qubits is obtained as the target state. Fortunately, thanks to the inherent symmetry of stabilizers, the desired ground state is protected from the noise due to the finite speed of evolution even if the energy gap vanishes.

In our models, we encode an individual qubit of the cluster state with a logical qubit of several spin-1/2 particles. We then establish the quantum correlations, i.e., *stabilizers*, of the cluster state in the initial state, which is also the ground state with a large energy gap protection. Hence, it tolerates a relatively high temperature. However, the initial state is not useful for the MBQC, since it is outside the logical subspace where logical qubits are encoded. We will show that these cluster-state correlations are protected during the entire adiabatic evolution, which is the key to our proposal. In this manner, the target or final state is a cluster state of a logical qubit, which can also be converted into a cluster state of spin-1/2 particles via single-qubit measurements.

3.2 General protocol

We encode each qubit of the cluster state in n spin-1/2 particles as

$$|0\rangle_j = \otimes_{m=1}^{n} |\uparrow\rangle_{j,m}, \quad |1\rangle_j = \otimes_{m=1}^{n} |\downarrow\rangle_{j,m}. \tag{3.1}$$

Here, the jth logical qubit is encoded in spin-1/2 particles $\{(j,m) : m = 1, 2, \ldots, n\}$, and $|\uparrow\rangle_{j,m}$ ($|\downarrow\rangle_{j,m}$) is the eigenstate of the Pauli operator $\sigma_{j,m}^z$ with the eigenvalue $+1$ (-1). These logical states are stabilized by operators $\{\sigma_{j,1}^z \sigma_{j,m}^z\}$, i.e., logical states are common eigenstates of these operators with eigenvalue $+1$. Pauli operators of the jth logical qubit are

$$X_j = \prod_{m=1}^{n} \sigma_{j,m}^x \text{ and } Z_j = \sigma_{j,1}^z. \tag{3.2}$$

This encoding has been used for constructing a perturbative model of the cluster state [36].

The cluster state is the common eigenstate with eigenvalue +1 of cluster-state stabilizers [15, 20, 21] $S_j = X_j \prod_{i\in nb(j)} Z_i = \prod_{m=1}^{n} \sigma_{j,m}^{x} \prod_{i\in nb(j)} \sigma_{i,1}^{z}$, where $nb(j)$ is the set of nearest neighboring logical qubits of the jth logical qubit. Hence, on the spin-1/2-particle level, the cluster state is stabilized by $\{S_j\}\cup\{\sigma_{j,1}^{z}\sigma_{j,m}^{z}\}$. By noticing that a product of stabilizers is also a stabilizer, cluster-state stabilizers can be rewritten as $S_j^{\{m_{j,i}\}} = S_j \prod_{i\in nb(j)} \sigma_{i,1}^{z}\sigma_{i,m_{j,i}}^{z} = \prod_{m=1}^{n} \sigma_{j,m}^{x} \prod_{i\in nb(j)} \sigma_{i,m_{j,i}}^{z}$, where $\{m_{j,i}\}$ is a string of numbers satisfying $1 \leq m_{j,i} \leq n$. If a state is stabilized by $\{S_j^{\{m_{j,i}\}}\} \cup \{\sigma_{j,1}^{z}\sigma_{j,m}^{z}\}$ for any choice of $\{m_{j,i}\}$, the state is the cluster state. This cluster state of logical qubits can be converted into a cluster state of physical qubits by measuring σ^x of arbitrary $n-1$ physical qubits of each logical qubit. Therefore, this cluster state of logical qubits is a universal resource for the MBQC.

To obtain the cluster state via adiabatic cluster-state concentration, we consider a Hamiltonian of $N \times n$ spin-1/2 particles in the form

$$H = H_0 + \lambda V, \tag{3.3}$$

where $H_0 = \sum_{j=1}^{N} h_j$ with $h_j = -J\sum_{m=1}^{n} \sigma_{j,m}^{z}\sigma_{j,m+1}^{z}$, where $\sigma_{j,n+1}^{z} = \sigma_{j,1}^{z}$, and J is the coupling constant of Ising interactions. Here, V denotes some two-body interactions that satisfy the following conditions:

1. V commutes with a set of cluster-state stabilizers $\{S_j^{\{m_{j,i}\}}\}$ corresponding to one choice of $\{m_{j,i}\}$; and

2. When the interaction strength λ is nonzero, degenerate ground states are split. As the result, H has a unique ground state with a finite energy gap above it.

Our protocol of cluster-state concentration includes two steps: 1) cooling the system with a nonzero λ to the ground state; 2) adiabatically switching off λ. In the adiabatic limit, the final state is the cluster state of logical qubits up to some single-particle Pauli operations.

This protocol relies on the set of cluster-state stabilizers $\{S_j^{\{m_{j,i}\}}\}$ that are conserved quantities for any value of λ, i.e., $[H, S_j^{\{m_{j,i}\}}] = 0$, $\forall\lambda$. We would like to remark that H_0 commutes with $S_j^{\{m_{j,i}\}}$. Hence, the unique ground state of H for any nonzero λ is the common eigenstate of cluster-state stabilizers. We suppose corresponding eigenvalues are $\{s_j^{\{m_{j,i}\}}\}$, where $s_j^{\{m_{j,i}\}} = +1$ or -1. Therefore, if the initial state is the ground state with a nonzero λ, the final state is still a common eigenstate of cluster-state stabilizers with the same eigenvalues.

For each logical qubit, $|0\rangle_j$ and $|1\rangle_j$ are degenerate ground states of h_j. The ground-state subspace of H_0 is 2^N-fold degenerate, which coincides with the subspace encoding logical qubits. During the adiabatic evolution, the state always remains in the ground state of the instantaneous Hamiltonian [17]. Thus, the final state is in the ground-state subspace of H_0, i.e. in the logical subspace.

Any state in the logical subspace is stabilized by $\{\sigma_{j,1}^z \sigma_{j,m}^z\}$. Therefore, the final state is the common eigenstate of $\{S_j^{\{m_{j,i}\}}\}$ and $\{\sigma_{j,1}^z \sigma_{j,m}^z\}$ with eigenvalues $\{s_j^{\{m_{j,i}\}}\}$ and $\{+1\}$, respectively. By performing single-particle Pauli operations $[(1+s_j^{\{m_{j,i}\}})\mathbb{1} + (1-s_j^{\{m_{j,i}\}})\sigma_{j,1}^z]/2$, the final state can be transformed into the cluster state of logical qubits.

When λ adiabatically approaches zero , the energy gap between the ground state and first-excited state vanishes, which usually implies one has to slow down the rate of change of λ to avoid any inadvertent excitation. Fortunately, in the degenerate subspace, i.e., the logical subspace, the cluster state is the only state with eigenvalues $\{s_j^{\{m_{j,i}\}}\}$. Similarly, the ground state is the only state with eigenvalues $\{s_j^{\{m_{j,i}\}}\}$ in all states split from the degenerate subspace. Therefore, the transitions between the ground states and other states split from the degenerate subspace are forbidden; i.e., one does not have to slow down the rate of change of λ, according to the vanishing energy gap, when $\lambda \to 0$.

In the following, we show that this generalized protocol is applied to three different models towards universal MBQC with fault-tolerant error correction in mind. We then focus on finding the energy gap of each model to prove that by cooling down the system unique, a ground state is feasible and that indeed our cluster-state concentration works as proposed.

3.3 1D Kitaev model

As discussed in the previous chapter, one-dimensional cluster state is not a resource state for universal MBQC. However, it helps to generate an arbitrary single-qubit gate [15, 20, 21], or can it be regarded as a quantum wire [40]. Our one-dimensional model inspires from the celebrated Kitaev's honeycomb model [41]. With closed boundary conditions, we arrive at the one-dimensional Kitaev model as shown in Fig.(3.1), and the system Hamiltonian is given by $H^{1D} = H_0^{1D} + \lambda V^{1D}$, where

$$H_0^{1D} = -J \sum_j \sigma_{j,1}^z \sigma_{j,2}^z, \tag{3.4}$$

$$V^{1D} = -\sum_j (\sigma_{j,1}^x \sigma_{j-2,2}^x + \sigma_{j,1}^y \sigma_{j-1,2}^y). \tag{3.5}$$

Here, each logical qubit, a grey oval shape in Fig.(3.1), is composed of a pair of spin-1/2 particles. The ground state is nondegenerate with a finite energy gap when $0 < \lambda < J/2$ [41]. We note that, for each plaquette j [see Fig.(3.1)], there

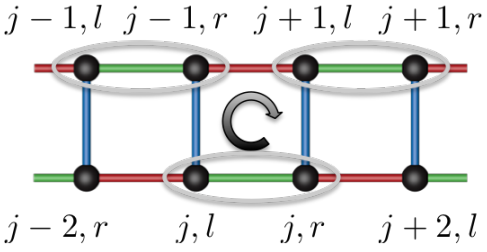

FIGURE 3.1: One-dimensional Kitaev model, where black circles represent spin-1/2 particles, red bonds denote $\sigma^x\sigma^x$, blue bonds denote $\sigma^y\sigma^y$, and green bonds are $\sigma^z\sigma^z$ two nearest neighbored interactions. j,l, and j,r label two physical qubits belonged to the logical qubit j (the grey oval shape).

is a conserved quantity

$$W_j = \sigma^x_{j,1}\sigma^x_{j,2}\sigma^z_{j-1,2}\sigma^z_{j+1,1}, \tag{3.6}$$

i.e., $[H^{1D}, W_j] = 0$. The conserved quantity is given by $W_j = S_j^{\{m_{j,i}\}}$ with $m_{j,j-1} = 2$ and $m_{j,j+1} = 1$. Therefore, the Hamiltonian H^{1D} satisfies the form Eq.(3.3). Since W_j's commute with each other, they can be diagonalized simultaneously with eigenvalues $w_j = \pm 1$, thus allowing us to partition the total Hilbert space into invariant subspaces of H^{1D}. We proceed to show that H^{1D} has the unique ground state locating in the subspace with $w_j = +1$, $\forall j$.

Using the Jordan-Wigner transformation:

$$\sigma^+_{ij} = 2\left[\prod_{j'<j}\prod_{i'}\sigma^z_{i'j'}\right]\left[\prod_{i'<i}\sigma^z_{i'j}\right]c^\dagger_{ij}, \tag{3.7}$$

$$\sigma^z_{ij} = 2c^\dagger_{ij}c_{ij} - 1, \tag{3.8}$$

we arrive at

$$\begin{aligned} H^{1D} =& \lambda \sum_{\text{x-bonds}} (c^\dagger - c)_r (c^\dagger + c)_l - \lambda \sum_{\text{y-bonds}} (c^\dagger + c)_l (c^\dagger - c)_r \\ & - J \sum_{\text{z-bonds}} (2c^\dagger c - 1)_l (2c^\dagger c - 1)_r. \end{aligned} \tag{3.9}$$

Let us introduce the Majorana fermions

$$A_r = (c - c^\dagger)_r / i, \qquad B_r = (c + c^\dagger)_r \tag{3.10}$$

for the right sites and

$$B_l = (c - c^\dagger)_l/i, \qquad A_l = (c + c^\dagger)_l \tag{3.11}$$

for the lefts. By substituting them back into $H^{1\mathrm{D}}$, we have

$$H^{1\mathrm{D}} = -i\left[\sum_{\text{x-bonds}} \lambda A_r A_l - \sum_{\text{y-bonds}} \lambda A_l A_r\right] - iJ \sum_{\text{z-bonds}} \alpha A_l A_r, \tag{3.12}$$

where

$$\alpha = iB_l B_r, \tag{3.13}$$

which is a conserved quantity [42] along the z-bond. We now relabel the Hamiltonian such that the summation over x, y and z-bonds becomes the summation over j^{th} sites as follow.

$$H^{1\mathrm{D}} = -i\sum_{j=1}^{N} \left[\lambda A_{j-1,r} A_{j+1,l} - \lambda A_{j,l} A_{j-1,r} + J\alpha A_{j,l} A_{j,r}\right], \tag{3.14}$$

where N is the total number of lattices or z-bonds. To diagonalize this Hamiltonian and find the ground state, we introduce a fermion in each z-bond by:

$$d_j = (A_{j,r} + iA_{j,l})/2, \qquad d_j^\dagger = (A_{j,r} - iA_{j,l})/2, \tag{3.15}$$

where A_r and A_l are the Majorana fermions on the right and left sites of a z-bond respectively. We substitute

$$A_{j,r} = d_j + d_j^\dagger, \qquad A_{j,l} = (d_j - d_j^\dagger)/i, \tag{3.16}$$

into the Eq(3.14). We arrive at

$$\begin{aligned} H^{\mathrm{1D}} &= \lambda\sum_j (d_{j-1}^\dagger + d_{j-1})(d_{j+1}^\dagger - d_{j+1}) + \lambda\sum_j (d_{j-1}^\dagger + d_{j-1})(d_j^\dagger - d_j) \\ &\quad + J\sum_j \alpha(2d_j^\dagger d_j - 1). \end{aligned} \tag{3.17}$$

The ground state for the fermions has $\alpha = 1$ everywhere [41]. For the bulk system, the exact solution for ground state is obtained by the Fourier transformation

$$d_j = \frac{1}{\sqrt{N}}\sum_q d_q e^{iqR_j}, \tag{3.18}$$

$$d_{j+1} = \frac{1}{\sqrt{N}}\sum_{q'} d_{q'} e^{iq'(R_j+a)}, \tag{3.19}$$

$$d_{j-1} = \frac{1}{\sqrt{N}}\sum_{q''} d_{q''} e^{iq''(R_j-a)}, \tag{3.20}$$

where a is the lattice parameter and R_j is the position coordinate of the j^{th} z-bond. We split H into three components to find its Fourier counterparts. For the x-component, we have

$$\begin{aligned} &\lambda\sum_j (d_{j-1}^\dagger + d_{j-1})(d_{j+1}^\dagger - d_{j+1}) \\ =&\lambda/N\sum_j \Bigg[\sum_{q',q''} \Big[e^{-i(q''+q')R_j} e^{i(q''-q')a} d_{q''}^\dagger d_{q'}^\dagger - e^{-i(q''-q')R_j} e^{i(q''+q')a} d_{q''}^\dagger d_{q'} \\ +&\ e^{-i(q'-q'')R_j} e^{-i(q''+q')a} d_{q''} d_{q'}^\dagger - e^{-i(-q''-q')R_j} e^{i(-q''+q')a} d_{q''} d_{q'}\Big]\Bigg] \\ =&\lambda\sum_q \left[e^{2iqa} d_q^\dagger d_{-q}^\dagger - e^{2iqa} d_q^\dagger d_q + e^{-2iqa} d_q d_q^\dagger - e^{-2iqa} d_q d_{-q}\right]. \end{aligned} \tag{3.21}$$

Similarly, for the y-component, we have

$$\begin{aligned}&\lambda\sum_j(d_{j-1}^\dagger+d_{j-1})(d_j^\dagger-d_j)\\=&\lambda\sum_q\left[e^{iqa}d_q^\dagger d_{-q}^\dagger-e^{iqa}d_q^\dagger d_q+e^{-iqa}d_qd_q^\dagger-e^{-iqa}d_qd_{-q}\right].\end{aligned}\tag{3.22}$$

The z-component is

$$J\sum_j(2d_j^\dagger d_j-1)=J\sum_q(2d_q^\dagger d_q-1).\tag{3.23}$$

By putting all the three pieces together, we have our final Hamiltonian as

$$H^{\mathrm{1D}}=\sum_q\left[\epsilon_qd_q^\dagger d_q+\frac{i\Delta_q}{2}(d_q^\dagger d_{-q}^\dagger+\mathrm{H.c.})\right],\tag{3.24}$$

where

$$\epsilon_q=2J-4\lambda\cos(2qa),\tag{3.25}$$

$$\Delta_q=4\lambda\sin(2qa).\tag{3.26}$$

After the Bogoliubov transformation, the Hamiltonian is diagonalized and the quasi-particle excitation is obtained and given by

$$E_q=\sqrt{\epsilon^2+\Delta_q^2}.\tag{3.27}$$

For the case when $|J_z|>|J_x|+|J_y|>0$, we can clearly see that $\epsilon_q=\Delta_q\neq0$ and thus $E_q\neq0$. Hence, the system is gapped.

Since W_j's are conserved quantities, the evolution is restricted to the $w_j = +1$ subspace. Therefore, the energy gap that protects the adiabatic evolution is always nonzero. The excitation spectrum is obtained by mapping [43] the original Hamiltonian H^{1D} into p-wave Fermi superfluid representation, where the energy gap between the ground state and the first excited state is $\Delta E^{1D} = 2J - 4\lambda$. With this energy gap, we first cool our system down to its ground state with nonzero λ as elaborated in the general protocol section. We then adiabatically switch off λ so that the final state is in the ground-state subspace of H_0^{1D}, stabilized by $W_j = X_j Z_{j-1} Z_{j+1}$, Eq.(3.6), yielding our 1D cluster state.

3.4 2D Kitaev-like model

To qualify for a resource state of the universal MBQC, we need a two-dimensional resource state, to accommodate for the single- and two-qubit gates. Following the one-dimensional cluster state, we propose a two-dimensional Kitaev-like model

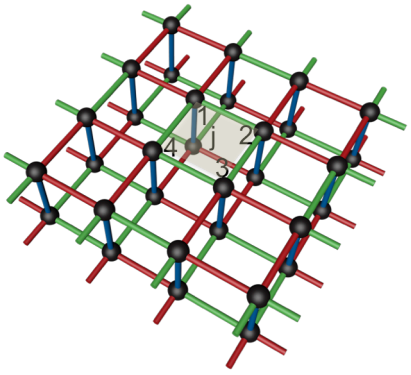

FIGURE 3.2: Two-dimensional Kitaev-like model, where black circles represent spin-1/2 particles, red bonds denote $\sigma_i^x \sigma_j^x$ interactions, blue bonds denote $\sigma_i^y \sigma_j^y$ interactions, and green bonds are $\sigma_i^z \sigma_j^z$ interactions where i and j label two corresponding spin-1/2 particles.

[see Fig.(3.2)] that satisfies the form of Eq.(3.3). The Hamiltonian of the two-dimensional model reads $H^{2\mathrm{D}} = H_0^{2\mathrm{D}} + \lambda V^{2\mathrm{D}}$, where

$$H_0^{2\mathrm{D}} = -J \sum_{\mathbf{j}} \sum_{\langle \mu,\mu' \rangle} \sigma^z_{\mathbf{j},\mu} \sigma^z_{\mathbf{j},\mu'}, \tag{3.28}$$

$$V^{2\mathrm{D}} = -\sum_{\langle \mathbf{j},\mathbf{j}' \rangle} \sum_{\mu} (\sigma^x_{\mathbf{j},\mu} \sigma^x_{\mathbf{j}',\mu_r} + \sigma^y_{\mathbf{j},\mu} \sigma^y_{\mathbf{j}',\mu_b}). \tag{3.29}$$

Each logical qubit, denoted by a green plaquette in Fig.(3.2), is composed of four physical spin-1/2 particles. Here, $\mathbf{j} = (j_1, j_2)$ is the coordinate of a logical qubit, $\langle \mu, \mu' \rangle$ labels two connected spin-1/2 particles which belong to the same logical qubit located at the position $\mathbf{j}$, $\langle \mathbf{j}, \mathbf{j}' \rangle$ denotes two connected logical qubits, and μ_r (μ_b) denotes the spin-1/2 particle connected with particle $(\mathbf{j}, \mu)$ via a red (blue) bond [see Fig.(3.2)]. For each logical qubit, there is a cube associated with a conserved quantity

$$W_{\mathbf{j}} = \sigma^x_{\mathbf{j},1} \sigma^x_{\mathbf{j},2} \sigma^x_{\mathbf{j},3} \sigma^x_{\mathbf{j},4} \times \sigma^z_{\mathbf{j}'+\mathbf{e_2},\mathrm{nb}(\mathbf{j},1)} \sigma^z_{\mathbf{j}'+\mathbf{e_1},\mathrm{nb}(\mathbf{j},2)} \sigma^z_{\mathbf{j}'-\mathbf{e_2},\mathrm{nb}(\mathbf{j},3)} \sigma^z_{\mathbf{j}'-\mathbf{e_1},\mathrm{nb}(\mathbf{j},4)}, \tag{3.30}$$

where $\mathbf{e_1}$ and $\mathbf{e_2}$ correspond to two unit vectors in the 3D Cartesian coordinate system. In addition, different $W_{\mathbf{j}}$'s commute with each other and also with the Hamiltonian, i.e., $[H^{2\mathrm{D}}, W_{\mathbf{j}}] = 0$. This model is nonintegrable. Thus, we cannot obtain the exact analytical energy gap. However, using standard perturbation technique [see Appendix A], we arrive at an effective Hamiltonian

$$H_{\mathrm{eff}}^{2\mathrm{D}} = \mathrm{const.} - (\lambda^6/1536 J^5) \sum_{\mathbf{j}} W_{\mathbf{j}}, \tag{3.31}$$

with an approximate energy gap of $\Delta E^{2D} \simeq \lambda^6/768J^5$. We anticipate a larger gap for larger λ, even if the perturbation is no longer valid. The 2D cluster state is then obtained following the same preparation procedure as the 1D cluster state.

3.5 3D square lattice model

A resource state in three dimensions is desirable since there is fault-tolerance quantum error correction scheme [44–46] that can be used to correct any inadvertent error during the quantum computations. In this section, we show the 3D square lattice model [see Fig.(3.3) (a)] has the unique ground state with an energy gap at $\lambda \neq 0$. Moreover, we provide some system operating parameters and conditions at which such system becomes a good resource state for the universal MBQC with built-in fault-tolerant quantum error correction schemes.

The Hamiltonian of the 3D square lattice model is given by $H^{3D} = H_0^{3D} + \lambda V^{3D}$, where

$$H_0^{3D} = -J \sum_j \sum_{\langle \mu,\mu' \rangle} \sigma^z_{(j,\mu)} \sigma^z_{(j,\mu')}, \text{ and} \tag{3.32}$$

$$V^{3D} = -\sum_j \sum_{\mu=1}^{4} \sigma^x_{(j,\mu)} \sigma^z_{\mathrm{nb(j,\mu)}}. \tag{3.33}$$

Each logical qubit j, a grey circle with four black circles in Fig.(3.3) (a), is encoded in four spin-1/2 particles and, there exists a unique analytic ground state after a controlled-phase unitary transformation ($\mathcal{CZ}$) on every bond [47, 48],

i.e., $\mathcal{H}^{3D} = (\mathcal{CZ})H^{3D}(\mathcal{CZ}) = \sum_j H_j^{3D}$, where $H_j^{3D} = [-J\sum_{\langle\mu,\mu'\rangle}\sigma^z_{(j,\mu)}\sigma^z_{(j,\mu')} - \lambda\sum_{\mu=1}^4\sigma^x_{(j,\mu)}]$. For each plaquette j, we notice there exists local conserved quantities

$$W_j^{\text{loc}} = (\mathcal{CZ})W_j(\mathcal{CZ}) = \prod_{\mu=1}^{4}\sigma^x_{(j,\mu)}, \tag{3.34}$$

such that W_j^{loc}'s commute with each other as well as with the Hamiltonian, i.e., $[H_j^{3D}, W_j^{\text{loc}}] = 0$. Since each jth plaquette is independent of each other, we have $\Delta E^{3D} = 2\sqrt{2J^2 + 2\lambda^2 + 2\sqrt{J^4+\lambda^4}} - 2\sqrt{J^2+\lambda^2} - 2J$, the energy gap [48] between its unique ground state and first excited state. This energy gap, [see Fig.(3.4)], ensures cooling the system to its unique ground state. This initial ground state of the time-dependent Hamiltonian $H_j^{3D}(\lambda(t))$ remains an approximate ground state of the Hamiltonian throughout the entire evolution as long as the rate of change of λ is sufficiently slow satisfying the adiabatic condition [17]. We also note that the stabilizers W_j^{loc}'s, Eq.(3.34), stabilize the

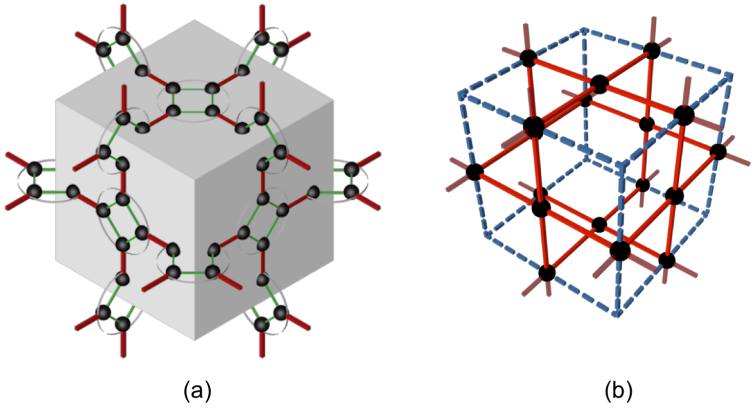

FIGURE 3.3: (a) Three-dimensional square lattice model, where black circles represent spin-1/2 particles, red bonds denote $\sigma_i^x\sigma_j^z$ interactions, and green bonds are $\sigma_i^z\sigma_j^z$ interactions where i and j are labels of two nearest-neighbor spin-1/2 particles. Here, a grey circle with four spin-1/2 particles is a logical qubit. (b) Equivalent model in a logical subspace, where four physical qubits bonded by $\sigma_i^z\sigma_j^z$ are taken as a single logical qubit, a black circle. Red colored $\sigma_i^x\sigma_j^z$ interactions remain the same, while the dashed box represents a unit square lattice.

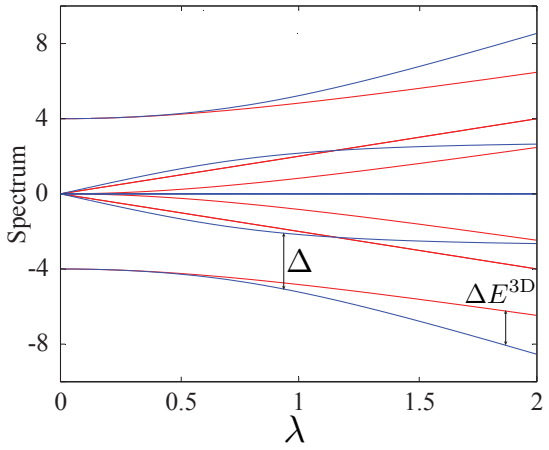

FIGURE 3.4: Energy spectrum of the 3D square lattice Hamiltonian H_j^{3D} versus the coupling λ. Energy eigenstates with eigenvalue +1 (eigenvalue -1) of the stabilizer, Eq.(3.34), are plotted in blue (red) solid lines.

instantaneous ground state throughout the adiabatic evolution ($t : 0 \to \tau$) since $[H_j^{3D}, W_j^{loc}] = 0$. Moreover, there exists a larger energy gap Δ within the subspace with eigenvalue +1 of the stabilizer that in turn allows us to apply a constant λ switching rate even though $\Delta E^{3D} \to 0$, where H^{3D} has many degenerate ground states. Thanks to the adiabatic evolution and the local stabilizers W_j^{loc}'s, we can concentrate our initially prepared ground states to computationally useful cluster states.

3.5.1 Error and feasibility

In the numerical simulation of the 3D cluster state concentration process, we consider a Hamiltonian of the form $H_j^{3D}(t) = H_{j0}^{3D} + \lambda(t)V_j^{3D}$, where $\lambda \to 0$ as $t : 0 \to \tau$ ($\tau = \lambda_0/v$ and $\lambda(t) = \lambda_0 - vt$). In this subsection, we provide some physical insights towards 3D cluster state concentration with feasible physical parameters that might help to guide experimental realization. As such, we prepare a thermal

state as the initial state, $\rho(0) = \mathcal{Z}^{-1}e^{-H_j^{3D}(0)/T}$, where $\mathcal{Z} = \mathrm{tr}e^{-H_j^{3D}(0)/T}$ and T is the temperature of the system setting the Boltzmann's constant to unity. The ground state without evolution [see Fig.(3.5) (inset)] corresponds to the case of a perturbative expansion [36]. With our adiabatic concentration process, the three different evolution times (τ = 5, 7, and 10) give rise to 3 orders of magnitude higher operating temperature compared to the no-evolution case. An important observation adduced from Fig.(3.5) is that the longer the evolution time, the higher the temperature, at which the system ground state can be prepared and the larger phase space region where standard fault-tolerant error correction schemes can be implemented to correct for possible errors.

Here, we further investigate errors origin of the 3D model from its geometrical nature, since it is well-known that the topological fault-tolerant quantum computing can be used to apply quantum error correction during the course of quantum

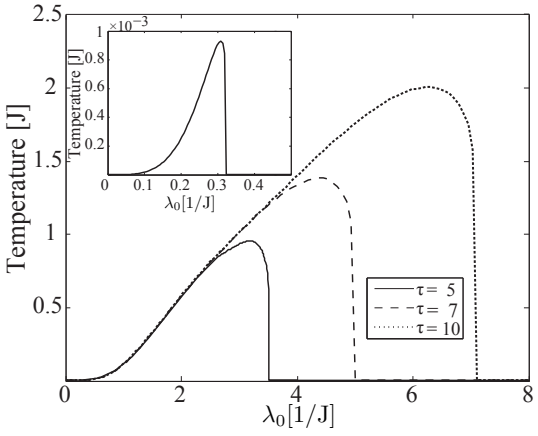

FIGURE 3.5: Phase diagram which shows, in temperature and initial coupling λ_0 space, the lines below which an initial thermal state after the adiabatic evolution is a resource state for fault-tolerent MBQC because the areas enclosed by the lines represent regions with less than 3% total phase-flip errors while the outer areas are regions with more than 3% total phase-flip errors. Solid line in the inset figure corresponds to the ground state without evolution while solid, dashed and dotted lines correspond to the ground state with evolution time τ = 5, 7, and 10 respectively.

computations as long as the average total phase-flip errors $E_\varsigma = P_Z + 4P_{C_1} + 2P_{C_2}$ of individual logical qubit in the 3-D model is 3% or less [44–46]. Errors on each square lattice in the final state can be expressed by a superoperator

$$E = F(\mathbb{1}) + P_Z \left(\sum_{k=1}^{4} [Z_k] \right) + \frac{P_{C_1}}{2} \left(\sum_{m \leftrightarrow l=1}^{4} [Z_l Z_m] \right) + \frac{P_{C_2}}{2} ([Z_1 Z_3] + [Z_2 Z_4]), \quad (3.35)$$

where F refers to fidelity, P_Z refers to local phase-flip errors, P_{C_1} refers to correlated errors type-1, $m \leftrightarrow l$ means the sites m and l are graphically connected, P_{C_2} refers to correlated errors type-2 [see Fig.3.7], F, P_Z, P_{C_1}, P_{C_2} are functions of their respective arguments, and a superoperator satisfies $\mathcal{O}[\rho] = \mathcal{O}\rho\mathcal{O}^\dagger$.

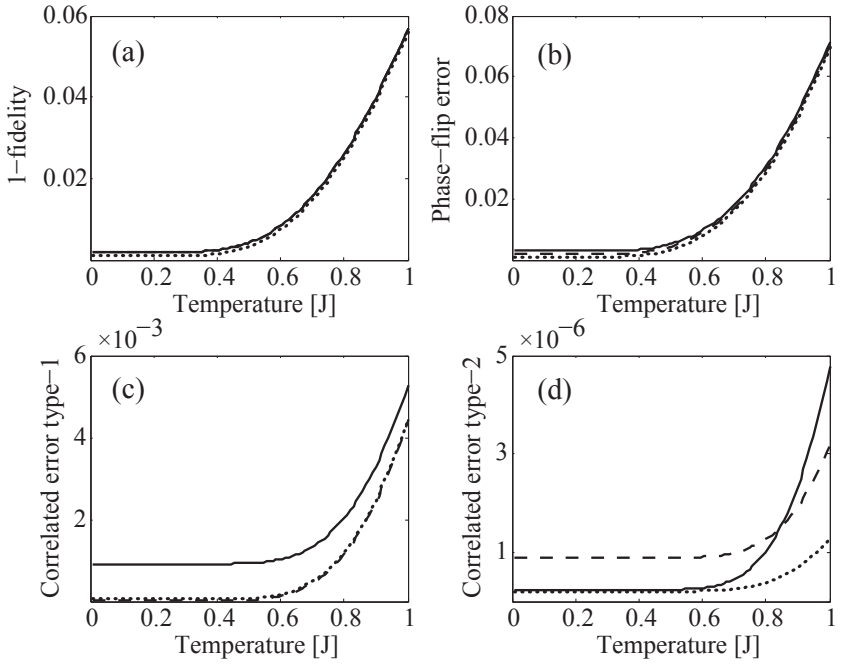

FIGURE 3.6: (a) Imperfection (1-fidelity) versus temperature plot. (b) Total phase-flip error (E_ς) versus temperature plot. (c) Correlated error type-1 (P_{C_1}) versus temperature plot. (d) Correlated error type-2 (P_{C_2}) versus temperature plot. Solid, dashed and dotted lines represent the evolution with $\tau = 5$, 7 and 10 respectively with $\lambda_0 = 2.5$.

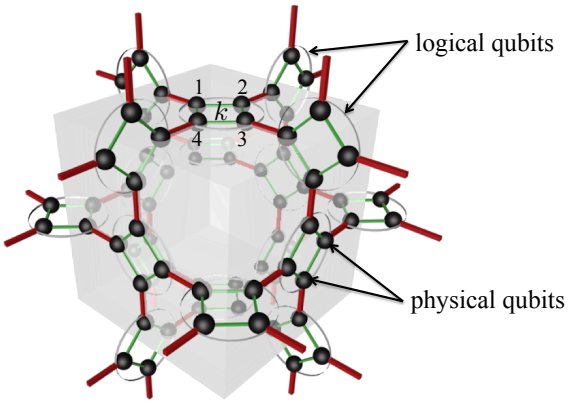

FIGURE 3.7: An elementary cubic lattice in the three-dimensional square lattice model. A grey circle of four spin-1/2 particles connected by four green bonds denotes a logical qubit. Numbers 1, 2, 3 and 4 label four physical qubits located inside the k logical qubit.

The efficiency and effectiveness of the fault-tolerance quantum computation depend not only on P_Z, which is estimated in Fig.(3.5), but also on correlated errors P_{C_1} and P_{C_2} among neighboring logical qubits. Here, we demand $P_{C_1}+P_{C_2} \ll P_Z$ so that the conclusion that we have adduced from Fig.(3.5) is valid. From the numerical evidence shown in Fig.(3.6) (b-d), it is clear that the above mentioned requirement is fulfilled in all the three different evolution times. Moreover, we see that halving temperature from $T = 1 \to 0.5$ for $\tau = 5, 7, 10$ reduces the total phase-flip errors by about one order of magnitude [see Fig.(3.6) (b)].

3.5.2 Sequential adiabatic switch-off

As proposed earlier on, we are required to turn-off all the nearest-neighbor interactions during our adiabatic cluster state concentration. However, it seems that this constraint is not a good way towards a scalable quantum computing, since the size of our resource state is bounded by decoherence rate of the logical qubits. However, in this subsection, we show that not all the interactions need

to be switched off. In fact, we can switch them off sequentially just before local measurement is performed on individual qubits. To be precise, the 3D system is initially prepared or cooled down to its unique ground state, which is not a computational resource state. We then adiabatically switch off $\lambda_{(j,\mu)}$'s for each logical qubit j one at a time. By doing so, we drive the jth logical qubit state into a computational resource state at the end of the adiabatic evolution. We then perform measurement onto this resource state. After the measurement of the jth logical qubit, Hamiltonian of the fully connected logical qubits in the residual Hamiltonian

$$
\begin{aligned}
H_{\rm res}^{\rm 3D} \;=\; & \sum_{k}^{N-5}[-J\sum_{\mu\leftrightarrow\mu'}\sigma^{z}_{(k,\mu)}\sigma^{z}_{(k,\mu')}-\sum_{\mu=1}^{4}\lambda_{(k,\mu)}\sigma^{x}_{(k,\mu)}\sigma^{z}_{nb(k,\mu)}](\text{f.c}) \\
& +\sum_{m\in nb(j)}^{4}[-J\sum_{\xi\leftrightarrow\xi'}\sigma^{z}_{(m,\xi)}\sigma^{z}_{(m,\xi')}-\sum_{\xi,(m,\xi)\nleftrightarrow(j,\mu)}^{3}\lambda_{(m,\xi)}\sigma^{x}_{(m,\xi)}\sigma^{z}_{nb(m,\xi)}](\text{p.c}),
\end{aligned}
\tag{3.36}
$$

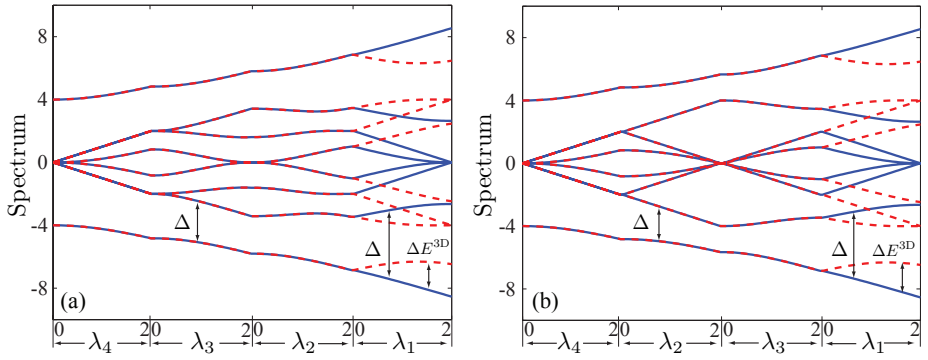

FIGURE 3.8: Energy spectrum of the 3-D square lattice Hamiltonian $H_j^{\rm 3D}$ versus the coupling λ's while (a) the surrounding logical qubit-1, 2, 3, and 4 and (b) the surrounding logical qubit-1, 3, 2, and 4 [see Fig. 3.7] are disconnected in sequential adiabatic manner where λ_1, λ_2, λ_3 and λ_4 are coupling constants between the central jth logical qubit and the surrounding logical qubit-1, 2 ,3 and 4 respectively. Energy eigenstates with eigenvalue +1 (eigenvalue -1) of the stabilizer are plotted in blue solid (red dashed) lines. Each λ is adiabatically tuned from 2 to 0 as in Fig.(3.4).

is still gapped (with ΔE^{3D}) as before and the four neighboring partially connected ones are no more protected by the gap. Here, N is the total number of logical qubits, $(m, \xi) \nleftrightarrow (j, \mu)$ means the physical qubit ξ belonged to the mth logical qubit is not graphically connected to the physical qubit μ belonged to the jth logical qubit and $nb(j)$ means neighbour of the jth logical qubit. From this observation, we draw attention that after every consumption of a resource state, there could be some other partially connected (p.c.) logical qubits located on a boundary between measured logical qubits and fully connected (f.c.) ones. These partially connected ones should be measured immediately or treated as redundant and discarded. Moreover, adiabatically switching off λ's of the jth qubit from the bulk does not couple instantaneous ground states with excited states because there is no level crossing in the energy spectra [see Fig.(3.8)], and this can be done monotonically in time due to the presence of larger energy gap Δ in the subspace defined by stabilizers throughout the entire adiabatic evolution. Specifically, from Fig.(3.8), we note that the ground state subspace with $+1$ eigenvalue of the stabilizers has non-zero energy gap $\Delta > \Delta E^{3D} > 0$ when λ's are being adiabatically turned off in succession.

With all the properties described above, our model enjoys an energy gap protection similar to the AKLT resource state [25]. The most important advantage with our proposal is that we are able to create cluster states of spin-1/2 particles with just nearest-neighbor two-body interactions.

Chapter 4

Outlook and conclusion

> "*The good thing about science is that it's true whether or not you believe in it*".
>
> — Neil deGrasse Tyson

Our proposal is not limited to the three models discussed so far and it can also be applied to other models such as the Bartlett and Rudolph's 2D hexagonal lattice [36], and the Kitaev's 2D honeycomb model [41]. However, the error correction threshold for the 2D cluster states [49–51] is believed to be much lower than that of 3D cluster states [44–46]. Thus, we are more interested in the implementation of our protocol in generating 3D cluster states. Our proposal benefits from an energy gap protection similar to that of the AKLT resource state [25] since the interactions can be switched off sequentially. Also, our models have a close connection with condensed matter models.

It is interesting to explore some future possible directions in this work. The central result of our current work is that we could overcome the no-go theorem

regarding the impossibility of a cluster state as a ground state of a two-body nearest-neighbor interaction Hamiltonian. Clearly aside from perturbation, we have shown that it is possible to obtain the desired highly entangled resource via adiabatic evolution. Other methods for obtaining the highly desired entangled resources is by projecting the ground states of higher dimensional systems through appropriate projective measurements or obtaining larger cluster states through a series of fusion rules or operations [52]. At this end, we have listed some open questions to be addressed in the foreseeable future.

- We have numerically studied the robustness of the concentration process for 3D cluster state with temperature using a thermal state as an initial state. It is known that quantum systems are highly influenced by the environment. It would therefore be interesting to extend the study to the effects of open system on the evolution using appropriate Master equations [53]. How does the errors propagate under open system dynamics? Moreover, one could also study the effects of non-Markovianity of such systems on the effectiveness of fault tolerance.

- For adiabatic evolution, the time needed to achieve adiabaticity is notoriously difficult to compromise. There is often a trade-off between decoherence of qubits and the time needed to maintain some adiabaticity. However, there are "short-cuts" in adiabatic quantum computation and it is interesting to invesigate if such "short-cuts" [54–57] are useful for our systems.

- In our study, we have restricted our model to simple Heisenberg interactions. However, there are many other nearest-neighbor models, like the Kagome lattice or Hubbard-type models, which are more appropriate for some solid state systems. We need to study more two-body nearest-neighbor Hamiltonians to compare and see their differences and similarities between different systems under our proposal.

- We note that there have been several methods that have been proposed to overcome the no-go theorem. It would be intersting to study these methods more carefully and see if one could combine some of these technqiues for a more robust way of creating the cluster states. In particular, there have been several studies on a robust coupling procedure that could couple small cluster or graph state arrays into bigger structures. This approach could also be investigated via an adiabatic method [52, 58].

In summary, we have proposed a means to create cluster states of spin-1/2 particles with just nearest-neighbor two-body interactions via adiabatic evolution, which could be experimentally realized with existing technology.

Bibliography

[1] Michael A Nielsen and Isaac L Chuang. *Quantum computation and quantum information*. Cambridge university press, 2010.

[2] Peter W Shor. Algorithms for quantum computation: Discrete logarithms and factoring. In *Foundations of Computer Science, 1994 Proceedings., 35th Annual Symposium on*, pages 124–134. IEEE, 1994.

[3] Lov K Grover. Quantum mechanics helps in searching for a needle in a haystack. *Physical review letters*, 79(2):325, 1997.

[4] David Cory and Todd Heinrichs. Nuclear magnetic resonance approaches to quantum information processing and quantum computing. *A Quantum Information Science and Technology Roadmap, v2.0*, 2004.

[5] Dave Wineland and Todd Heinrichs. Ion trap approaches to quantum information processing and quantum computing. *A Quantum Information Science and Technology Roadmap, v2.0*, 2004.

[6] Carlton Caves and Todd Heinrichs. Neutral atom approaches to quantum information processing and quantum computing. *A Quantum Information Science and Technology Roadmap, v2.0*, 2004.

[7] Michael Chapman and Todd Heinrichs. Cavity qed approaches to quantum information processing and quantum computing. *A Quantum Information Science and Technology Roadmap, v2.0*, 2004.

[8] Alexandre Blais, Ren-Shou Huang, Andreas Wallraff, SM Girvin, and R Jun Schoelkopf. Cavity quantum electrodynamics for superconducting electrical circuits: An architecture for quantum computation. *Physical Review A*, 69 (6):062320, 2004.

[9] Thomas Orlando and Todd Heinrichs. Superconducting approaches to quantum information processing and quantum computing. *A Quantum Information Science and Technology Roadmap, v2.0*, 2004.

[10] Paul Kwiat, Gerard J Milburn, and Todd Heinrichs. Optical approaches to quantum information processing and quantum computing. *A Quantum Information Science and Technology Roadmap, v2.0*, 2004.

[11] Robert Clark, David Awschalom, David DiVincenzo, P Chris Hammel, Duncan Steel, K. Birgitta Whaley, and Todd Heinrichs. Solid state approaches to quantum information processing and quantum computing. *A Quantum Information Science and Technology Roadmap, v2.0*, 2004.

[12] Seth Lloyd, P Chris Hammel, and Todd Heinrichs. "unique"qubit approaches to quantum information processing and quantum computing. *A Quantum Information Science and Technology Roadmap, v2.0*, 2004.

[13] David P DiVincenzo. The physical implementation of quantum computation. *arXiv preprint quant-ph/0002077*, 2000.

[14] Los alamos national security. *A Quantum Information Science and Technology Roadmap, v2.0*, 2004.

[15] Robert Raussendorf and Hans J Briegel. A one-way quantum computer. *Physical Review Letters*, 86(22):5188, 2001.

[16] Alexei Kitaev and Chris Laumann. Topological phases and quantum computation. *arXiv preprint arXiv:0904.2771*, 2009.

[17] Edward. Farhi, Jeffrey Goldstone, Sam Gutmann, and Michael Sipser. Quantum computation by adiabatic evolution. *arXiv preprint quant-ph/0001106*, 2000.

[18] Thi Ha Kyaw, Ying Li, and Leong-Chuan Kwek. Measurement-based quantum computation on two-body interacting qubits with adiabatic evolution. *Physical review letters*, 113(18):180501, 2014.

[19] Maarten Van den Nest, Akimasa Miyake, Wolfgang Dür, and Hans J Briegel. Universal resources for measurement-based quantum computation. *Physical Review Letters*, 97(15):150504, 2006.

[20] Robert Raussendorf, Daniel E Browne, and Hans J Briegel. Measurement-based quantum computation on cluster states. *Physical review A*, 68(2): 022312, 2003.

[21] Hans J Briegel, Daniel E Browne, Wolfgang Dür, Robert Raussendorf, and Maarten Van den Nest. Measurement-based quantum computation. *Nature Physics*, 5(1):19, 2009.

[22] Robert Raussendorf, Sergey Bravyi, and Jim Harrington. Long-range quantum entanglement in noisy cluster states. *Physical Review A*, 71(6):062313, 2005.

[23] David Jennings, Andrzej Dragan, Sean D Barrett, Stephen D Bartlett, and Terry Rudolph. Quantum computation via measurements on the low-temperature state of a many-body system. *Physical Review A*, 80(3):032328, 2009.

[24] Michael A Nielsen. Cluster-state quantum computation. *Reports on Mathematical Physics*, 57(1):147, 2006.

[25] Gavin K Brennen and Akimasa Miyake. Measurement-based quantum computer in the gapped ground state of a two-body hamiltonian. *Physical Review Letters*, 101(1):010502, 2008.

[26] Tzu-Chieh Wei, Ian Affleck, and Robert Raussendorf. Two-dimensional affleck-kennedy-lieb-tasaki state on the honeycomb lattice is a universal resource for quantum computation. *Physical Review A*, 86(3):032328, 2012.

[27] Tzu-Chieh Wei, Ian Affleck, and Robert Raussendorf. Affleck-kennedy-lieb-tasaki state on a honeycomb lattice is a universal quantum computational resource. *Physical Review Letters*, 106(7):070501, 2011.

[28] Akimasa Miyake. Quantum computational capability of a 2d valence bond solid phase. *Annals of Physics*, 326(7):1656, 2011.

[29] Xie Chen, Bei Zeng, Zheng-Cheng Gu, Beni Yoshida, and Isaac L Chuang. Gapped two-body hamiltonian whose unique ground state is universal for

one-way quantum computation. *Physical Review Letters*, 102(22):220501, 2009.

[30] Jianming Cai, Akimasa Miyake, Wolfgang Dür, and Hans J Briegel. Universal quantum computer from a quantum magnet. *Physical Review A*, 82 (5):052309, 2010.

[31] Leandro Aolita, Augusto J Roncaglia, Alessandro Ferraro, and Antonio Acín. Gapped two-body hamiltonian for continuous-variable quantum computation. *Physical Review Letters*, 106(9):090501, 2011.

[32] Ying Li, Daniel E Browne, Leong Chuan Kwek, Robert Raussendorf, and Tzu-Chieh Wei. Thermal states as universal resources for quantum computation with always-on interactions. *Physical Review Letters*, 107(6):060501, 2011.

[33] Keisuke Fujii and Tomoyuki Morimae. Topologically protected measurement-based quantum computation on the thermal state of a nearest-neighbor two-body hamiltonian with spin-3/2 particles. *Physical Review A*, 85(1):010304, 2012.

[34] Akimasa Miyake. Quantum computation on the edge of a symmetry-protected topological order. *Physical Review Letters*, 105(4):040501, 2010.

[35] Kihwan Kim, M-S Chang, S Korenblit, R Islam, EE Edwards, JK Freericks, G-D Lin, L-M Duan, and C Monroe. Quantum simulation of frustrated ising spins with trapped ions. *Nature*, 465(7298):590, 2010.

[36] Stephen D Bartlett and Terry Rudolph. Simple nearest-neighbor two-body hamiltonian system for which the ground state is a universal resource for quantum computation. *Physical Review A*, 74(4):040302, 2006.

[37] Edward Farhi, Jeffrey Goldstone, Sam Gutmann, Joshua Lapan, Andrew Lundgren, and Daniel Preda. A quantum adiabatic evolution algorithm applied to random instances of an np-complete problem. *Science*, 292(5516): 472, 2001.

[38] Andrew M Childs, Edward Farhi, and John Preskill. Robustness of adiabatic quantum computation. *Physical Review A*, 65(1):012322, 2001.

[39] Marcelo Sarandy and Daniel Lidar. Adiabatic quantum computation in open systems. *Physical review letters*, 95(25):250503, 2005.

[40] Daivd Gross, Jens Eisert, Norbert Schuch, and David Perez-Garcia. Measurement-based quantum computation beyond the one-way model. *Physical Review A*, 76(5):052315, 2007.

[41] Alexei Kitaev. Anyons in an exactly solved model and beyond. *Annals of Physics*, 321(1):2, 2006.

[42] Xiao-Yong Feng, Guang-Ming Zhang, and Tao Xiang. Topological characterization of quantum phase transitions in a spin-1/2 model. *Physical review letters*, 98(8):087204, 2007.

[43] Han-Dong Chen and Zohar Nussinov. Exact results of the kitaev model on a hexagonal lattice: spin states, string and brane correlators, and anyonic

excitations. *Journal of Physics A: Mathematical and Theoretical*, 41(7): 075001, 2008.

[44] Robert Raussendorf, Jim Harrington, and Kovid Goyal. Topological fault-tolerance in cluster state quantum computation. *New Journal of Physics*, 9 (6):199, 2007.

[45] Robert Raussendorf, Jim Harrington, and Kovid Goyal. A fault-tolerant one-way quantum computer. *Annals of Physics*, 321(9):2242, 2006.

[46] Robert Raussendorf and Jim Harrington. Fault-tolerant quantum computation with high threshold in two dimensions. *Physical Review Letters*, 98 (19):190504, 2007.

[47] Tom Griffin and Stephen D Bartlett. Spin lattices with two-body hamiltonians for which the ground state encodes a cluster state. *Physical Review A*, 78(6):062306, 2008.

[48] Daniel Klagges and Kai Phillip Schmidt. Constraints on measurement-based quantum computation in effective cluster states. *Physical Review Letters*, 108(23):230508, 2012.

[49] Robert Raussendorf. Measurement-based quantum computation with cluster states. *International Journal of Quantum Information*, 7(06):1053, 2009.

[50] Ashley M Stephens, Austin G Fowler, and Lloyd C L Hollenberg. Universal fault tolerant quantum computation on bilinear nearest neighbor arrays. *arXiv preprint quant-ph/0702201*, 2007.

[51] Ashley M Stephens and Zachary W E Evans. Accuracy threshold for concatenated error detection in one dimension. *Physical Review A*, 80(2): 022313, 2009.

[52] Simon C Benjamin, Daniel E Browne, Joe Fitzsimons, and John JL Morton. Brokered graph-state quantum computation. *New Journal of Physics*, 8(8): 141, 2006.

[53] Heinz-Peter Breuer and Francesco Petruccione. *The theory of open quantum systems*. Oxford university press, 2002.

[54] MV Berry. Transitionless quantum driving. *Journal of Physics A: Mathematical and Theoretical*, 42(36):365303, 2009.

[55] Xi Chen, I Lizuain, A Ruschhaupt, D Guéry-Odelin, and JG Muga. Shortcut to adiabatic passage in two-and three-level atoms. *Physical review letters*, 105(12):123003, 2010.

[56] S Ibánez, Xi Chen, E Torrontegui, JG Muga, and A Ruschhaupt. Multiple schrödinger pictures and dynamics in shortcuts to adiabaticity. *Physical review letters*, 109(10):100403, 2012.

[57] Adolfo del Campo. Shortcuts to adiabaticity by counterdiabatic driving. *Physical review letters*, 111(10):100502, 2013.

[58] Liang Jiang, Jacob M Taylor, Anders S Sørensen, and Mikhail D Lukin. Distributed quantum computation based on small quantum registers. *Physical Review A*, 76(6):062323, 2007.

[59] Julia Kempe, Alexei Kitaev, and Oded Regev. The complexity of the local hamiltonian problem. *SIAM Journal on Computing*, 35(5):1070, 2006.

Appendix A

Perturbation Theory

The use of perturbation theory in the present context is to obtain the spectrum of a Hamiltonian $\widetilde{H} = H + V$, where H is an unperturbed Hamiltonian while V is a small perturbation. Our main objective is to approximate the spectrum of $\widetilde{H}$ as close as possible and we can then claim that the spectrum of H_{eff}, which is the effective Hamiltonian, provides the required answer.

Let us assume H has a zero eigenvalue with an associated eigenspace, whereas all other eigenvalues are greater than $\triangle \gg \|V\|$, where $\triangle$ is the assumed energy spectral gap around some cutoff eigenvalue $\lambda_* \in \mathbb{R}$ on the spectrum of H. Let λ_j, $|\psi_j\rangle$ ($\widetilde{\lambda}_j, |\widetilde{\psi}_j\rangle$) be the eigenvalues and the eigenvectors of H ($\widetilde{H}$) respectively. From now on, everything related to the perturbed Hamiltonian $\widetilde{H}$ is marked with tilde. We define the resolvent of $\widetilde{H}$ as

$$\widetilde{G}(z) = \left(zI - \widetilde{H}\right)^{-1} = \sum_j \left(z - \widetilde{\lambda}_j\right)^{-1} |\widetilde{\psi}_j\rangle\langle\widetilde{\psi}_j|, \tag{A.1}$$

and its usefulness comes from the fact that $\widetilde{G}$ has poles at $z = \widetilde{\lambda}_j$ and the poles can be preserved under projections while eigenvalues are usually not. Similarly, we define the resolvent of H as

$$G(z) = (zI - H)^{-1} = \sum_j (z - \lambda_j)^{-1} |\psi_j\rangle\langle\psi_j|. \tag{A.2}$$

Definition: Let $\mathcal{H} = \mathcal{L}_+ \oplus \mathcal{L}_-$, where $\mathcal{L}_+$ is the space spanned by eigenvectors of H with eigenvalues $\lambda \geq \lambda_*$ and $\mathcal{L}_-$ is the space spanned by eigenvectors of H with eigenvalues $\lambda < \lambda_*$. Let $\Upsilon_\pm$ be corresponding projection operator onto $\mathcal{L}_\pm$. For an operator V on $\mathcal{H}$, we define operator $V_{++} = V|_{\mathcal{L}_+} = \Upsilon_+ V \Upsilon_+$ on $\mathcal{L}_+$ and similarly $V_{--} = V|_{\mathcal{L}_-}$. We also define $V_{+-} = \Upsilon_+ V \Upsilon_-$ as an operator from $\mathcal{L}_-$ to $\mathcal{L}_+$, and similarly for $V_{-+} = \Upsilon_- V \Upsilon_+$. Finally, we define self-energy function as

$$\Sigma_-(z) = zI_- - \widetilde{G}_{--}^{-1}(z). \tag{A.3}$$

To derive the expression for H_{eff}, we first express $\widetilde{G}$ in terms of G as

$$\widetilde{G} = \left(G^{-1} - V\right)^{-1} = \begin{pmatrix} G_{++}^{-1} - V_{++} & -V_{+-} \\ -V_{-+} & G_{--}^{-1} - V_{--} \end{pmatrix}^{-1},$$

since G is block diagonal in the representation of $\mathcal{H} = \mathcal{L}_+ \oplus \mathcal{L}_-$. Using the block matrix identity

$$\begin{pmatrix} A & B \\ C & D \end{pmatrix}^{-1} = \begin{pmatrix} (A - BD^{-1}C)^{-1} & -A^{-1}B(D - CA^{-1}B)^{-1} \\ -D^{-1}C(A - BD^{-1}C)^{-1} & (D - CA^{-1}B)^{-1} \end{pmatrix}, \tag{A.4}$$

we find

$$\widetilde{G}_{--} = \left(G_{--}^{-1} - V_{--} - V_{-+} \left(G_{++}^{-1} - V_{++} \right)^{-1} V_{+-} \right)^{-1}. \tag{A.5}$$

With the help of the series expansion $(I-Y)^{-1} = I+Y+Y^2+\cdots$ and Eq.(A.2), we have the expression for the self-energy function in terms of the perturbation V as

$$\begin{aligned}
\Sigma_-(z) &= zI_- - G_{--}^{-1} + V_{--} + V_{-+} \left(G_{++}^{-1} - V_{++} \right)^{-1} V_{+-} \\
&= H_{--} + V_{--} + V_{-+} \left(G_{++}^{-1} - V_{++} \right)^{-1} V_{+-} \\
&= H_{--} + V_{--} + V_{-+} G_{++} \left(I_+ - V_{++} G_{++} \right)^{-1} V_{+-} \\
&= H_{--} + V_{--} + V_{-+} G_{++} V_{+-} + V_{-+} G_{++} V_{++} G_{++} V_{+-} + \\
&\quad V_{-+} G_{++} V_{++} G_{++} V_{++} G_{++} V_{+-} + \cdots
\end{aligned} \tag{A.6}$$

Proof:

1. By definition $\widetilde{G}(z) = (zI - \widetilde{H})^{-1}$, the eigenvalues of $\widetilde{H}|_{\widetilde{\mathcal{L}}_-}$ appear as poles in $\widetilde{G}$.

2. These poles also appear as poles of $\widetilde{G}_{--}$.

3. z is a pole of $\widetilde{G}_{--}$ if and only if it is an eigenvalue of $\Sigma_-(z)$.

4. If we assume H_{eff}, which we obtain by taking non-constant leading orders in $\Sigma_-(z)$, is close to $\Sigma_-(z)$, then any eigenvalue of $\Sigma_-(z)$ must be close to an eigenvalue of H_{eff}. Thus, eigenvalues of H_{eff} must be close to those of $\widetilde{H}|_{\widetilde{\mathcal{L}}_-}$.

Hence, we take Eq.(A.6) as H_{eff} as long as the condition $\triangle \gg \|V\|$ is satisfied. For the detailed proof, one may refer to Ref.[59].

A.1 Perturbative study in the 2D Kitaev-like model

A.1.1 Configuration 1

Here, we directly apply the mathematical results and notations from the previous section, while V^{2D} term in the 2D model Hamiltonian is taken as a perturbative term. The perturbative results are listed below.

1. $H_{\text{eff}}^{(0)} = H_{--} = E_0 = -NJ_z$, where N is the number of unit cells.
2. $H_{\text{eff}}^{(1)} = V_{--} = 0$.
3. $H_{\text{eff}}^{(2)} = V_{-+}G_{++}V_{+-} = \text{const.}$
4. $H_{\text{eff}}^{(3)} = V_{-+}G_{++}V_{++}G_{++}V_{+-} = \text{const.}$
5. $H_{\text{eff}}^{(4)} = V_{-+}G_{++}V_{++}G_{++}V_{++}G_{++}V_{+-} = \text{const.}$

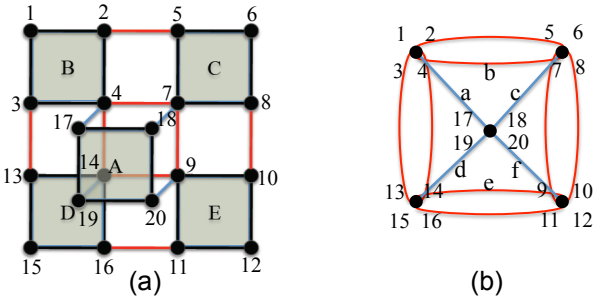

FIGURE A.1: (a) Configuration 1 of the 2D cluster state, derived from Fig.(3.2), with a single logical qubit in the upper layer is shown. (b) The same figure (a) is shown in the logical subspace. The numbers 1-20 label physical spins.

6. $H_{\text{eff}}^{(5)} = V_{-+}G_{++}V_{++}G_{++}V_{++}G_{++}V_{++}G_{++}V_{+-} = \text{const.}$

7. $H_{\text{eff}}^{(6)} = \text{const} - \frac{J_x^2 J_y^4}{1536 J_z^5} \sum_p \sigma^y_{17(\text{p})}\sigma^y_{18(\text{p})}\sigma^y_{19(\text{p})}\sigma^y_{20(\text{p})}\sigma^z_{4(\text{p})}\sigma^z_{7(\text{p})}\sigma^z_{9(\text{p})}\sigma^z_{14(\text{p})}$,

where $\frac{1}{1536} = 16 \cdot \frac{-1}{4096} + 16 \cdot \frac{1}{4096} + 8 \cdot \frac{-1}{6144} + 8 \cdot \frac{1}{6144} + 8 \cdot \frac{-1}{8192} + 8 \cdot \frac{1}{8192} + 8 \cdot \frac{1}{12288}$, which we obtain from flipping of eight spins along diagonal two blue colored lines followed by flipping of the four spins along the red line that connect the two blue lines with rectangular symmetry. Hence, the effective Hamiltonian is

$$\begin{aligned} H_{\text{eff}}^{(6)} &= \text{const} - \frac{J_x^2 J_y^4}{1536 J_z^5} \sum_{\text{p}} \sigma^y_{17(\text{p})}\sigma^y_{18(\text{p})}\sigma^y_{19(\text{p})}\sigma^y_{20(\text{p})}\sigma^z_{4(\text{p})}\sigma^z_{7(\text{p})}\sigma^z_{9(\text{p})}\sigma^z_{14(\text{p})} \\ &= \text{const} - \frac{J_x^2 J_y^4}{1536 J_z^5} \sum_{\text{p}} (W_p)_{\text{eff}}. \end{aligned} \tag{A.7}$$

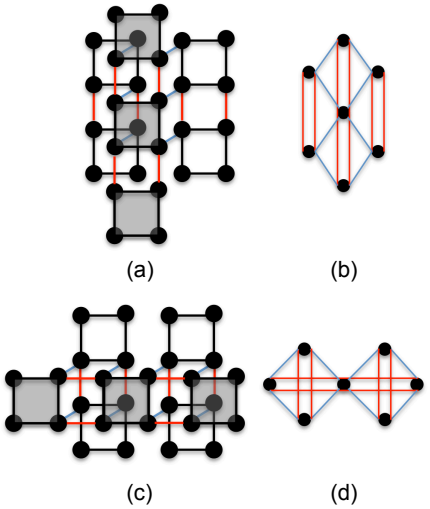

FIGURE A.2: (a-c) Configurations 2 and 3 of the 2D cluster state, derived from Fig.(3.2), are shown. (b-d) show their respective configurations in the logical subspace.

A.1.2 Configuration 2 and 3

After going through the same mathmatical exercises as before, we arrive at the effective Hamiltonian of the configuratins shown in Fig.(A.2) as

$$H_{\text{eff}}^{(6)} = \text{const} - \frac{J_x^2 J_y^4}{3072 J_z^5} \sum_{\text{p}} (W_p)_{\text{eff}}. \tag{A.8}$$

Even though the two configurations in Fig.(A.2) are total difference, we get the same effective Hamiltonian. The deviation only comes in when we go to higher order perturbation.